*Journal of Statistical Physics, Vol. 54, Nos. 3/4, 1989*

# On the Symmetry-Breaking Bifurcation of Chaotic Attractors

**K. G. Szabó[1] and T. Tél[1]**

*Received August 9, 1988*

A new type of crisis is shown to exist in a broad class of systems (including the Lorenz model) which leads to an anomalous band splitting or to a symmetry-breaking bifurcation of the strange attractor, depending on the actual values of the control parameters. A piecewise linear model is used to understand the mechanism of this crisis and to obtain exact results.

**KEY WORDS:** Symmetry breaking; chaos; band splitting; crisis; piecewise linear map.

## 1. INTRODUCTION

Symmetry breaking is a common phenomenon in nature.[1] In the field of dynamical systems, the symmetry-breaking bifurcation of attractors is a subject of special interest. For limit cycles this phenomenon has been studied extensively,[2] especially in the Lorenz model.[3] Less is known about the symmetry breaking of chaotic attractors. A symmetry-recovering crisis has been discovered experimentally and modeled in ref. 4. Here we consider the symmetry breaking of strange attractors from another point of view in a more general class of systems and we show that a new type of crisis[5] may exist leading to an anomalous band splitting[6] or to a symmetry-breaking transition of the strange attractor, depending on the actual values of the parameters.

We investigate Lorenz-type systems characterized by the property that trajectories on the attractor pass close to a saddle point. This saddle has a two-dimensional stable and a one-dimensional unstable invariant manifold. Therefore, trajectories approaching the stable manifold may stay for an

[1] Institute for Theoretical Physics, Eötvös University, H-1088 Budapest, Puskin u. 5–7, Hungary.



0022-4715/89/0200-0925$06.00/0 

arbitrarily long time in the vicinity of the saddle and cause singularities in the form of the Poincaré map. Besides the standard Lorenz model, the Rikitake dynamo[7] and a model of Rössler[8] show similar behavior. Different approximate forms of the corresponding Poincaré map have been deduced[9–14] in the spirit of Shilnikov's method.[15] The most general version seems to be the one developed in ref. 13 (see also ref. 16), which yields the following map:

$$\begin{aligned} x' &= (-1 + a\,|x|^{\beta})\,\mathrm{sgn}(x) + cy\,|x|^{\delta} \\ y' &= (d + |x|^{\beta})\,\mathrm{sgn}(x) + by\,|x|^{\delta} \end{aligned} \tag{1.1}$$

where $x$ and $y$ denote suitably chosen coordinates on the Poincaré plane, and $a$, $b$, $c$, and $d$ are constant parameters. The exponents $\beta$ and $\delta$ can be expressed as the ratios of the eigenvalues of the linearized motion around the saddle point of the flow.[13] Due to the singularities of the map, the Jacobian is strongly position dependent:

$$J(x) = (ab - c)\,\beta\,|x|^{\beta+\delta-1} \tag{1.2}$$

The form (1.1) is exact in the vicinity of the point where the unstable manifold of the saddle intersects the Poincaré plane and can be considered to be a good approximation outside this region. Since the flow has been assumed to exhibit the symmetry of the Lorenz model, the map is invariant under the transformation

$$(x, y) \mapsto (-x, -y) \tag{1.3}$$

Therefore, the attractors of (1.1) must either be invariant under this transformation or appear in pairs of inverse images. In the latter case we speak about broken symmetry.

We have investigated numerically the chaotic attractors of the map (1.1) and their structural changes. The most concise description of the results can be given in the form of phase diagrams (Fig. 1) exhibiting regions of the parameter plane associated with different types of strange attractors at fixed values of the parameters $b$, $d$, $\beta$, and $\delta$. These regions are bounded by crisis lines. For a broad range of the exponents $\beta$ and $\delta$ a qualitatively similar behavior has been found. In all these cases the chaotic attractor undergoes a symmetry-breaking bifurcation. The region where a symmetry-broken attractor exists is bounded by three lines: by the continuation of a normal band-splitting curve ($n_1$ on Fig. 1), by a new type of crisis line ($a_2$), and, from below, by the line separating chaotic and regular behavior ($p$). Along another piece of the new crises line ($a_2$), another new

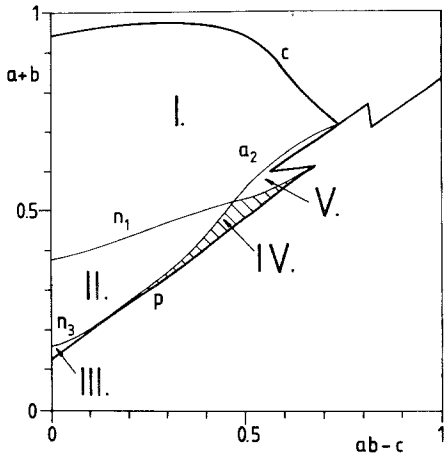


Fig. 1. Phase diagram of the map (1.1) with $\beta = 1.2$, $\delta = 0.2$, $b = -0.1$, $d = 0$. To be consistent with other diagrams, the $(ab - c, a + b)$ plane is shown. Beneath the curve $p$ stable periodic solutions are found; above the crisis line $c$ no finite stable attractor exists. The chaotic region between $p$ and $c$ is further divided as follows. I: symmetric 2-piece strange attractor; II and III: band-split symmetric 4- (8-) piece attractor; IV (shaded): 4-piece attractor with broken symmetry; V: anomalously split 6-piece symmetric attractor. For simplicity, the coexisting regular attractors and the periodic windows are not displayed.

phenomenon can be observed, an anomalous band splitting from a 2-piece to a 6-piece symmetrical strange attractor.

In order to understand these phenomena we turn to the investigation of a piecewise linear version of the original map.

This strategy has been successfully applied in several other problems. In the case of the Lozi map,[17] which is the piecewise linear approximation of Hénon's map,[18] exact calculations have been performed[19–22] leading to a qualitative understanding of the phase diagrams. The Lozi map has turned out to be a useful model also for studying the scaling structure of strange attractors[22] and the behavior in the Hamiltonian limit.[23] A discontinuous piecewise linear map[24,25] and different versions of the baker's transformation[26–31] have provided examples with exactly calculable fractal characteristics. Piecewise linear approximations have helped the understanding of deterministic diffusion[32] and of certain properties of the circle map.[33]

From our point of view the main advantage of using an approximation like this is the fact that the strange attractor and the invariant manifolds of two-dimensional piecewise linear maps can be constructed analytically with arbitrary precision. Therefore, the specification of crisis lines by means of numerical methods—which is, in general, quite

complicated and time consuming—can be avoided. On the other hand, as suggested by the example of the Lozi and Hénon maps, a qualitatively similar behavior is expected in the original map and in its piecewise linear version. Thus, we believe that the mechanism leading to the existence of the new crisis line of symmetry breaking and anomalous band splitting can be understood through the piecewise linear problem.

The paper is organized as follows. The piecewise linear map and a few properties of it are introduced in Section 2. Then, the method of constructing invariant manifolds in an analytical way is summarized in Section 3. Usual crisis lines such as that of the boundary crisis[5] or of band splittings are specified in Section 4. The above-mentioned novel features are discussed in Section 5. Further interesting properties—the existence of a chaotic repellor[34] (replacing the attractor in certain regions of parameter space) and the fractal dimension of the strange sets—are studied in the Appendix. An outlook based upon the results obtained for both the original map and the piecewise linear one is given in Section 6.

## 2. THE MODEL

In the following we consider the piecewise linear version of the map (1.1) obtained for $\beta = 1$, $\delta = 0$:

$$\begin{aligned} x' &= ax + cy - \operatorname{sgn}(x) \\ y' &= x + by + d \operatorname{sgn}(x) \end{aligned} \tag{2.1}$$

By the linear transformation $(x, y) \to (x, [y + dx]/[1 + (a-b)d - cd^2])$ the third term on the right-hand side of the second equation can be eliminated. Henceforth, we use these transformed coordinates, i.e., we study (2.1) with $d = 0$.

The trace ($A$) and the Jacobian ($J$) of this map are obtained as

$$A = a + b \tag{2.2}$$

and

$$J = ab - c \tag{2.3}$$

respectively. The forthcoming results and expressions become simpler by using parameters $A$, $J$, and $b$ rather than $a$, $b$, and $c$. For the same reason phase diagrams showing the behavior of the piecewise linear map (2.1) at fixed values of $b$ will be displayed in the next sections on the $(J, A)$ plane.

The map may possess two fixed points, $\mathbf{z}_+$ and $\mathbf{z}_-$, the solutions of the linear equations

$$\mathbf{z}_+ = T_+(\mathbf{z}_+), \qquad \mathbf{z}_- = T_-(\mathbf{z}_-) \tag{2.4}$$

Here the vector notation, $\mathbf{z} = (x, y)$ and $\mathbf{z}' = T(\mathbf{z})$, of (2.1) has been used, and $T_+$ ($T_-$) stands for the restriction of $T$ to the half-plane $x > 0$ ($x < 0$). The symmetry of (2.1) implies $\mathbf{z}_+ = -\mathbf{z}_-$ and, consequently,

$$\begin{aligned} x_+ &= \frac{1-b}{A-1-J} = -x_- \\ y_+ &= \frac{1}{A-1-J} = -y_- \end{aligned} \tag{2.5}$$

Since $\operatorname{sgn}(x_+) = +1$ has been assumed, these fixed points exist only if

$$\frac{1-b}{A-1-J} > 0 \tag{2.6}$$

holds.

The period-2 points are obtained from the equation

$$\mathbf{z}^* = T^{(2)}(\mathbf{z}^*) \tag{2.7}$$

where $T^{(2)}$ is the twofold iterated map. Two of the solutions are just the fixed points $\mathbf{z}_+$ and $\mathbf{z}_-$. The remaining ones, $\mathbf{z}_{+-}$ and $\mathbf{z}_{-+}$, form a period-2 orbit with coordinates

$$\begin{aligned} x_{+-} &= \frac{1+b}{A+1+J} = -x_{-+} \\ y_{+-} &= \frac{-1}{A+1+J} = -y_{-+} \end{aligned} \tag{2.8}$$

In this case positivity of $x_{+-}$ has been assumed; thus

$$\frac{1+b}{A+1+J} > 0 \tag{2.9}$$

should hold.

We shall see that the map exhibits chaotic behavior when both

period-1 and period-2 points exist. Thus, we study the region of the parameter space where the inequalities

$$A > |1 + J| \tag{2.10a}$$

$$|b| < 1 \tag{2.10b}$$

are satisfied.

The stability of the fixed points is governed by the eigenvalues of the Jacobian. It is easy to see from (2.2) and (2.3) that these are

$$\lambda_{\pm} = [A \pm (A^2 - 4J)^{1/2}]/2 \tag{2.11}$$

The fixed points are stable if both $\lambda_+$ and $\lambda_-$ have real parts less then 1 in modulus. This holds if $A < 1 + J$ and $|J| < 1$ (see Fig. 2). The fixed points are unstable nodes or spirals if $|J| > 1$ and either $A < 1 + J$ or $A < -(1 + J)$ holds. If $A > |1 + J|$, which is just the condition (2.10a), the eigenvalues are real and $\lambda_+ > 1$ and $|\lambda_-| < 1$, i.e., the fixed points are hyperbolic.

The stability of the period-2 orbit is given by the eigenvalues of the Jacobian of the twofold iterated map $T^{(2)}$. Since the Jacobian of the

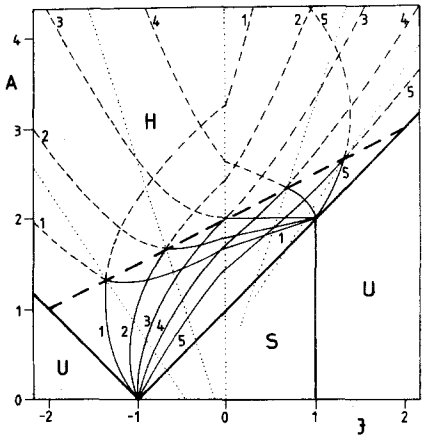


Fig. 2. Phase diagram for a map of type (2.1). Continuous heavy lines separate the regions of the $(J, A)$ parameter plane where all the periodic orbits of the map (2.1) are stable (S), unstable (U), and hyperbolic (H); the dashed heavy line corresponds to $\lambda_+ = 2$. These curves do not depend on $b$. The upper bound of the chaotic region [the function $A_c(J)$ of Section 4] is denoted by continuous thin curves for different values of $b$: (1) $b = -2/3$, (2) $b = -1/3$, (3) $b = 0$, (4) $b = 1/3$, (5) $b = 2/3$. In each cases the dotted lines of $\lambda_- = b$ are displayed as well. For the same values dashed lines show the lower bound $A_r(J)$ of the regions where chaotic repellors with regular double Cantor-set structure exist, as discussed in Appendix B.

original map is constant, these eigenvalues are $\lambda_+^2$ and $\lambda_-^2$. Similarly, the corresponding eigenvalues for an arbitrary orbit of period $n$ are $\lambda_+^n$ and $\lambda_-^n$. Consequently, the stability of all periodic orbits with real eigenvalues is the same. This implies that no stable periodic orbit can exist in the hyperbolic case (2.10a); thus any finite attractor must then be a chaotic (strange) one, and periodic windows cannot be present in the system.

## 3. THE STRUCTURE OF THE STRANGE ATTRACTOR

The unstable manifold of a periodic orbit can be obtained by determining small pieces of this manifold in (arbitrarily small) neighborhoods of the periodic points and by letting these pieces be mapped several times. The subsequent images will grow along the unstable manifold; thus, higher and higher order images of the original pieces will approximate the unstable manifold better and better. The stable manifold can be constructed in a similar way by using the inverted map instead of the original one.

This construction is difficult to perform in general cases, but is found to be simple and useful for piecewise linear maps.[20,24] We shall extend the method of ref. 24 in constructing the invariant sets of (2.1).

From the fixed point equations (2.4) one can derive the eigenvectors corresponding to the eigenvalues $\lambda_+^n$ and $\lambda_-^n$. They are

$$\mathbf{u}_\pm = (\lambda_\pm - b, 1) \tag{3.1}$$

respectively, independently of $n$. These eigenvectors yield the directions of the unstable and stable manifolds in the neighborhood of the point investigated. Due to the fact that the Jacobian matrix of our piecewise linear map is constant, the manifolds will consist of straight line segments running parallel to each other with the common slope $\lambda_\pm - b$.

The first steps in constructing $W_{+-}^u$, the unstable manifold of the period-2 cycle, is shown in a chaotic case on Fig. 3, where $C_0$ and $\bar{C}_0$ stand for the intersections of the first branches of $W_{+-}^u$ with the $y$ axis. The segment $\bar{C}_0\bar{H}$ is mapped onto $\bar{C}_1 H$, which is mapped further onto $\bar{C}_{1,1}\bar{H}$. Due to the symmetry, $C_0 H \to C_1\bar{H} \to C_{1,1}H$ also holds. Consequently, the first branches going through the period-2 points are $\bar{C}_1 C_{1,1}$ and $C_1\bar{C}_{1,1}$, so these branches are to be chosen as the initial segments for further iterations. The forthcoming iteration maps $\bar{C}_0\bar{C}_{1,1}$ onto $\bar{C}_{0,1}\bar{C}_{1,2}$, which lies in the lower half-plane, so its image will be *one* branch, $\bar{C}_{0,2}\bar{C}_{1,3}$. This new segment sticks into the upper half-plane, thus generating *two* new branches in the next step. From the branches of $W_{+-}^u$ obtained this way, further branches can be constructed by repeating the procedure several times.

Figure 3 also indicates the first branches of the stable manifolds $W_+^s$

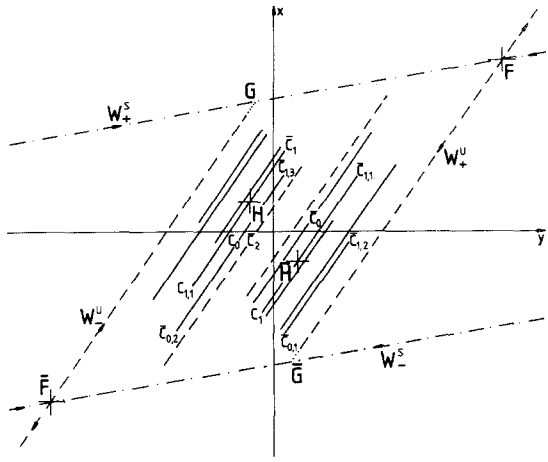


Fig. 3. The first four steps in constructing the branches of the unstable manifolds of the period-2 orbit lying within the parallelogram $FG\bar{F}\bar{G}$ ($a=1.85$, $b=0.25$, $c=-0.2375$, $A=2.1$, $J=0.7$). The fixed points $\mathbf{z}_+$, $\mathbf{z}_-$ and the period-2 points $\mathbf{z}_{+-}$, $\mathbf{z}_{-+}$ are denoted by $F$, $\bar{F}$, $H$, and $\bar{H}$, respectively (bar denotes inverted image). Mapping the first branch of $W^u_{+-}$, one obtaines the following branches: $\bar{C}_0\bar{C}_{1,1} \to \bar{C}_{0,1}\bar{C}_{1,2} \to \bar{C}_{0,2}\bar{C}_{1,3} \to$ two additional lines. Beginning with the branch $\bar{C}_1 C_{1,1}$, the construction yields the inverse images of these, belonging also to $W^u_{+-}$. The dashed lines represent the first two branches of $W^u_+$ and $W^u_-$, the unstable manifolds of the fixed points. The dash-dotted lines are the first branches of the stable manifolds $W^s_+$ and $W^s_-$.

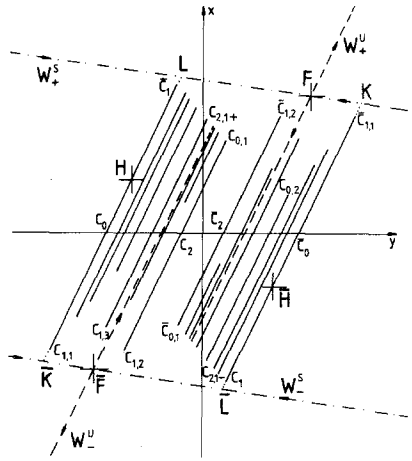


Fig. 4. The branches of $W^u_{+-}$ are located within the parallelogram $KL\bar{K}\bar{L}$ at $a=1.65$, $b=-0.25$, $c=0.2875$ ($A=1.4$, $J=-0.7$). The branches obtained up to the fourth step are $C_0C_{1,1} \to C_{0,1}C_{1,2} \to C_{0,2}C_{2,1-} \cup C_{2,1+}C_{1,3} \to$ further four branches. The inverted images of these lines are also indicated. Further notations are identical to those of Fig. 3.

and $W^s_-$ and the first two branches of the unstable manifolds $W^u_+$ and $W^u_-$ corresponding to the fixed points, constructed in a similar way. Further steps of the construction would convince us that the unstable manifold of the period-2 points runs among the branches of $W^u_+$ and $W^u_-$. Subsequent iterations of an arbitrary point lying between $W^s_+$ and $W^s_-$ thus approach $W^u_{+-}$. This illustrates that the parallelogram $FG\overline{FG}$ defined by the intersections of $W^s_+$, $W^s_-$ and the continuations of the first branches of $W^u_-$ and $W^u_+$ is a "trapping region" of an attractor. Since at this parameter values no stable finite periodic orbit can exist, this attractor will be a chaotic one. By this method, the basin of attraction can also be constructed; it is bounded by the branches of $W^s_+$ and $W^s_-$ connected with the preimages of the $y$ axis.

Figure 4 shows the unstable manifold of the period-2 orbit constructed in an analogous way for a topologically different case. There are two essential differences between Figs. 3 and 4. First, the fixed points lie now between the branches of $W^u_{+-}$, because the contraction rate $\lambda_-$ is negative. Thus, the "trapping parallelogram" is $KL\overline{KL}$ now, defined by the first branches of the stable manifolds of the fixed points and the continuations of the first branches of the unstable manifold of period-2 points. Second, the slope $\lambda_- - b$ of the stable manifold is negative.

In fact, there are four different topological structures, depending on the sign of $\lambda_-$ and the sign of the slope $(\lambda_- - b)$ of the stable manifolds. In all these cases, as Figs. 3 and 4 suggest, the chaotic attractor is the unstable manifold of the period-2 orbit (more precisely, the closure of it).

## 4. CRISIS CONFIGURATIONS

In this section we discuss what happens to the strange attractor while the parameters of the map are being varied.

As the stretching ratio $\lambda_+$ increases (by increasing the parameter $A$), the branches of the unstable manifold $W^u_{+-}$ become longer and longer. If $\lambda_+$ is big enough, heteroclinic points appear: the first branch of $W^s_+$ ($W^s_-$) and $W^u_{+-}$ intersect. The parallelogram $FG\overline{FG}$ of Fig. 3 or $KL\overline{KL}$ of Fig. 4 (according to the sign of $\lambda_-$) will then no longer be trapping regions, since almost all points of these quadrilaterals sooner or later will be mapped outside, and will then tend to infinity along $W^u_+$ or $W^u_-$.

In the critical situation of boundary crisis[5] the topmost points of the chaotic attractor just touch the first branch of the stable manifold $W^s_+$. This condition holds along a critical line $A_c(J)$ of the parameter plane. The function $A_c(J)$ can be calculated for all the topologically different cases discussed in the previous section. Here we give explicit formulas only for one case; others can be treated along similar lines.

If $\lambda_- < \min(0, b)$ (see Fig. 4), the topmost point of the attractor is $\bar{C}_1$. The coordinates of this point can be derived by taking into consideration that $\bar{C}_1$ is the image of $\bar{C}_0$, the intersection point of the $y$ axis and of the first branch of $W^u_{+-}$. The latter line goes through $\mathbf{z}_{-+}$ and has the slope of $\lambda_+ - b$ [see (3.1)]. Using Eqs. (2.8) and (2.1), a simple calculation yields

$$x_1 = \frac{b+1}{1+\lambda_-}, \qquad y_1 = \frac{b}{(1+\lambda_-)(\lambda_+ - b)} \tag{4.1}$$

for the coordinates of $\bar{C}_1$. The first branch of $W^s_+$ is given by the equation

$$x = (\lambda_- - b)\, y + 1/(\lambda_+ - 1) \tag{4.2}$$

as follows from (2.5) and (3.1). Substituting (4.1) into (4.2), the condition for the crisis is found to be

$$(\lambda_+ - 1)[(b+1)\,\lambda_+ - b(1+\lambda_-)] = (1+\lambda_-)(\lambda_+ - b) \tag{4.3}$$

yielding a piece of the $A_c(J)$ function. [For the special case $b=0$ this condition is equivalent to $A_c = 2(1+J)^{1/2}$.[24]]

The full $A_c(J)$ function can be obtained by joining the pieces corresponding to different cases. This function is plotted on Fig. 2 at

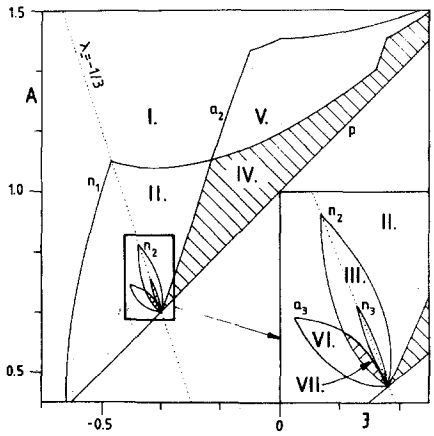


Fig. 5. A typical phase diagram of the map (2.1) at $b = -1/3$. The tips of the normal band-splitting lines $n_i$ are aligned along $\lambda_- = b$. The regions of the 2-, 4-, 8-piece symmetric attractors are assigned by I, II, and III. The line $a_2$ belongs to the homoclinic crisis of the period-4 points. The shaded region IV locates the symmetry-broken attractor with four pieces, while region V denotes the anomalously split 6-piece symmetric attractor (cf. Fig. 1). The boundary of the regions VI and VII, belonging to the symmetric 12-piece and the asymmetric 8-piece attractors, respectively, is $a_3$, the line of the homoclinic crises of period-8 orbit.

different values of $b$. Breakpoints appear on the line $\lambda_- = b$ ($c = 0$) and along $\lambda_- = 0$ ($J = 0$), dividing the parameter plane according to the cases mentioned above.

It is worth noticing that $\lambda_+ \leqslant 2$ is a condition for this heteroclinic crisis, as can be seen from Fig. 2. The equality can be fulfilled only if $\lambda_- = b$, i.e., if all the stable manifolds run parallel to the $y$ axis [see Eq. (3.1)]. In this case the map (2.1) is equivalent to the generalized baker's transformation as defined in refs. 27 and 31.

On the other hand, it is interesting to study what happens when parameter $A$ is decreased (see Fig. 5). The 2-piece attractor (like the ones on Figs. 3 and 4) splits into 4-, 8-, 16-, ...-piece attractors, i.e., a band-splitting sequence is observed.

Figure 6 shows the mechanism of band splitting. As the topmost point $P_0$ of the left-hand band gets *below* the second branch $\gamma$ of the stable manifold $W^s_{+-}$, its subsequent images $P_1$, $P_2$, $P_3$ also get below the corresponding branches $\alpha$, $\beta$, $\alpha$, while—due to the symmetry (1.3)—$\bar{P}_0$, $\bar{P}_1$, $\bar{P}_2$, and $\bar{P}_3$ will lie *above* the branches $\delta$, $\beta$, $\alpha$, and $\beta$, respectively. This way a gap arises around the period-2 points; the chaotic bands will not contain them any longer. In fact, the attractor is not the closure of $W^u_{+-}$, it is rather associated with $W^u_{++--}$, the unstable manifold of the period-4 point $\mathbf{z}_{++--}$. Band splitting is the consequence of the homoclinic crisis of the period-2 orbit and, simultaneously, the heteroclinic crisis with the unstable manifold of the period-4 orbit.

The investigation of higher-order band splittings is carried out in an analogous way. Equations for the different band-splitting crisis lines can be derived just like (4.3). Figure 5 shows the numerical solution of these up to the third bifurcation for a fixed value of $b$.

Along the line $\lambda_- = b$ the sequence of breakpoints where $2^n$-piece attractors split into $2^{n+1}$-piece ones happens to be at $\lambda_+ = \lambda_+^{(n)} \equiv 2^{1/2^n}$, yielding an explicit sequence converging to $\lambda_+ = 1$. ($\lambda_+^{(0)} = 2$ is just the boundary crisis situation.)

An infinite sequence of band splittings can be found only if one approaches the line $\lambda_+ = 1$ at $\lambda_- = b$. Along a general line of the parameter space, however, the periodic state is reached after a finite number of bifurcations. This phenomenon was first found in the case of the Lozi map[20]; an infinite band-splitting sequence was observed there only in the limit of extremely strong dissipation, $J \to 0$.

The map (2.1) also exhibits new, peculiar ways of changing the shape of the strange attractor, namely anomalous band splitting and symmetry-breaking transition.

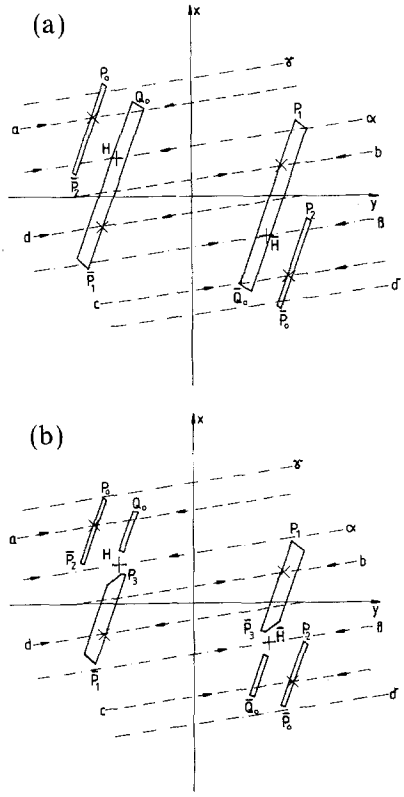


Fig. 6. (a) Above and (b) below the normal band-splitting crisis situation. $H$ and $\bar{H}$ are the period-2 points, the dash-dotted lines $\alpha$, $\beta$, $\gamma$, and $\delta$ are the branches of $W^s_{+\_}$. The dashed lines $a$, $b$, $c$, and $d$ are the first branches of $W^s_{++\_\_}$, the stable manifold of the period-4 points denoted by crosses. The attractor is located inside the bands. The bands are split into pieces by the period-2 points due to the disappearance of homoclinic intersections with $W^s_{+\_}$.

## 5. ANOMALOUS BAND SPLITTING AND SYMMETRY-BREAKING TRANSITION

In addition to the normal band-splitting curves, Fig. 5 shows other crisis lines as well. Figure 7 illustrates what happens when one crosses the line $a_2$. This curve intersects the line $n_1$ of normal homoclinic crisis of period-2 points and reaches $p$ at $\lambda_- = b$. Whether an anomalous band splitting or a symmetry-breaking transition occurs at a given point of $a_2$ depends on the actual position of this point. Below the normal band-splitting line $n_1$ a symmetry-breaking transition occurs, while above it an anomalous band splitting appears.

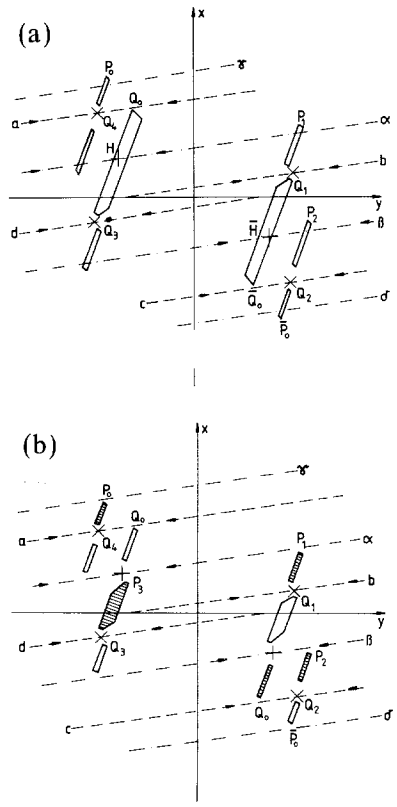


Fig. 7. (a) The structure of a symmetrical strange attractor anomalously split into six pieces. Gaps around the period-4 points arise because the bands do not intersect with the dashed branches of $W^s_{++--}$. (b) The shaded and nonshaded bands involve a pair of 4-piece attractors with broken symmetry which appears because the bands of the attractor intersect neither $W^s_{+-}$ nor $W^s_{++--}$. (Notation is identical to that of Fig. 6.)

Let us consider the latter case first, by comparing Figs. 6a and 7a. As the stretching ratio $\lambda_+$ is decreased, the topmost point $Q_0$ of the internal band on the left-hand side gets beneath the branch $a$ of the stable manifold $W^s_{++--}$ of the period-4 orbit, and $\bar{Q}_0$ gets above the branch $c$. New gaps appear around the period-4 points similarly to the way discussed in the previous section. The attractor is still (the closure of) the unstable manifold of the period-2 orbit, but, as Fig. 7b suggests, it does not contain the 4-cycle. Thus, the attractor has become a 6-piece one, since it lies now in separate pieces within the six "zones" bounded by the branches $a$, $b$, $c$, and $d$ of $W^s_{++--}$. We call this type of transition an anomalous band splitting, since the homoclinic intersections of the period-4 orbit disappear, while

those of the period-2 orbit still exist. This homoclinic crisis of the 4-cycle is accompanied by heteroclinic crises with the unstable manifolds of other periodic points.

We emphasize that the aforementioned crisis is caused by a new mechanism different from that of the normal band splitting. The line $a_2$ of Fig. 5 is obtained as the numerical solution of the equation describing this anomalous band splitting of period-4 points.

Figure 7b shows the situation arising when the parameters are changed so as to lie beneath both $n_1$ and $a_2$. Despite the gaps around period-2 and period-4 points, the resulting attractor is not an 8-piece one. The branches of the stable manifolds $W^s_{+-}$ and $W^s_{++--}$ of period-2 and period-4 orbits divide the basin of attraction into zones. These are of two kinds: those bounded by $W^s_{+-}$ from above and by $W^s_{++--}$ from below, and those bounded by $W^s_{++--}$ from above and by $W^s_{+-}$ from below. Zones of either kind are mapped now onto zones of the same type; for example, the zone between $\gamma$ and $a$ is mapped onto $\alpha$–$b$, and $d$–$\beta$ is mapped onto $a$–$\alpha$. Similarly, a chaotic trajectory is trapped into zones of one kind. It implies that the chaotic bands involve two distinct strange attractors. These sets, shaded differently on Fig. 7b, are asymmetric, being the inverse images of each other. The union of zones of a given type is the basin of attraction of the corresponding 4-piece asymmetric strange attractor.

Our argument is based upon the fact that $\lambda_- > b$ and $P_2$, the second image of the topmost point, lies on the lower half-plane. Under these circumstances, the absence of the homoclinic points of period-2 and period-4 symmetric orbits is the condition for the existence of chaos with broken symmetry (see Fig. 5).

For $\lambda_- < b$, a pair of 8-piece asymmetric attractors can be observed within region VII of Fig. 5. The lines $n_1$, $n_2$, and $a_3$ encircle regions of the parameter space where no homoclinic intersections of the respective period-2, -4, and -8 orbits exist. These symmetric cycles exist but do not belong to the strange attractor, since their stable manifolds, $W^s_{+-}$, $W^s_{++--}$, and $W^s_{++-+--+-}$, create two disjoint basins of attraction.

On the other hand, if $P_2$ lies on the upper half-plane, chaotic orbits will involve sequences keeping the same sign of the $x$ coordinates in three subsequent iterations. Thus, additional bands will appear on both sides of the attractor containing $\mathbf{z}_{+++---}$ and $\mathbf{z}_{---+++}$, the points of a new symmetric period-6 orbit. These bands may recover the symmetry by transferring orbits between zones of different type until $W^u_{+++---}$, the unstable manifold of this cycle, traverses the branches of $W^s_{+-}$ or $W^s_{++--}$. Detailed investigation shows that asymmetric chaotic attractors result only if homoclinic points of the period-6 orbit also disappear. (The upper boundary of region V on Fig. 5 is the line where anomalous gaps

appear around both $\mathbf{z}_{++--}$ and $\mathbf{z}_{+++---}$. The broken shape of the curve bounding regions IV and V is also due to this effect.)

Summarizing this section, the onset of chaos via symmetry breaking has proven to be typical in this piecewise linear discontinuous system. As the control parameter is decreased, unstable cycles become separated from the strange attractor by homoclinic crises, and the attractor splits into several pieces. If all the existing symmetric orbits lose their homoclinic points, their stable manifolds divide the formerly single basin of attraction into two symmetric pieces. These sets become the basins of two separate chaotic attractors which are the images of each other under the symmetry of the map (2.1).

## 6. CONCLUSIONS

Two dimensional dissipative maps described by analytic functions have typical properties depending on the value of the effective Jacobian $J \in (0, 1)$[35,36]: the infinite sequence of band splittings and the universal order in the crossings of periodic windows. In this paper we have shown that this universal behavior is changed drastically in discontinuous mappings occurring, e.g., in Lorenz-type systems. Due to the fact that the invariant manifolds of the periodic points of a system like this consist of countless disjoint branches rather than single connected curves of infinite length, the regular order of homo- and heteroclinic crises breaks down. When hyperbolic periodic orbits become separated from the chaotic attractor independently of the normal band-splitting order, anomalous band splittings arise. In discontinuous systems with symmetry, due to the numerous anomalous band splittings, strange attractors with broken symmetry may be found in large regions of the parameter space.

In order to illuminate the mechanism of these phenomena, we have investigated the structure of the chaotic attractor in the symmetric piecewise linear map (2.1). This is a simplified version of the map (1.1), where symmetry breaking was found to be a typical phenomenon in a wide range of the parameters $\beta$ and $\delta$. Since in our map the branches of the manifolds are straight line segments, we have succeeded in determining the lines of several crises on the phase diagram of the system.

On the basis of this simple example we expect the following scenario to be valid for general discontinuous symmetrical maps. The strange attractor undergoes a symmetry-breaking bifurcation whenever the heteroclinic intersections with the stable manifolds of the existing symmetric cycles disappear. In other words, when two asymmetric chaotic attractors collide simultaneously on the boundary separating their basins, a new symmetric attractor with double size arises as the union of the previous ones. This

mechanism is essentially the same as the one described in ref. 4 for continuous symmetrical maps. For discontinuous maps, however, a more complex behavior might result, such as the truncation of the infinite sequence of band splittings and the appearance of anomalous band splittings. These phenomena typically occur in the region of parameter space where the size of chaotic attractors is relatively small, that is, close to the onset of chaos.

Finally, we mention what happens when asymmetric perturbations are present. In this case the symmetrical pair of attractors is replaced by two coexisting nonsymmetrical ones, say $A$ and $A'$, with their basins separated by $B$, the stable manifold of a hyperbolic periodic orbit. As the control parameter changes, only one of the attractors, $A$, might collide with the boundary and undergo a boundary crisis and, if so, it becomes a repellor transferring the orbits from its former basin toward $A'$. $A'$ will collide with $B$ only if the parameter is further varied. Then an internal crisis happens to $A'$ since its size grows suddenly while its basin remains unchanged. The extended strange attractor will involve the orbit to which $B$ belongs. The reversed process can be interpreted as a generalization of the symmetry-breaking bifurcations of chaotic attractors.

## APPENDIX A. THE FRACTAL DIMENSION OF THE STRANGE ATTRACTOR

The strange attractor of the map (2.1) constructed in Section 3 has a nontrivial fractal dimension[37] $D$. Due to the simple structure of the map, it is possible to derive an exact expression for $D$ if $|\lambda_-| < 1/2$ is supposed. (The case $|\lambda_-| > 1/2$ is discussed separately at the end of this Appendix.) Our argument is based upon the idea of ref. 24, taking into consideration the more rigorous mathematical discussion of ref. 25.

The forthcoming discussion, which is first applied to the case $0 < \lambda_- < b$, $\lambda_- < 1/2$, is best followed on Fig. 8. The attractor is the closure of the unstable manifold $W^u_{+-}$ located within the "trapping parallelogram" $FG\bar{F}\bar{G}$. The smallest parallelogram of the ones covering the attractor and having sides parallel to the stable and unstable directions is denoted by $F_0G_0\bar{F}_0\bar{G}_0$. Let $\varepsilon_0$ be the width of this quadrilateral, i.e., the distance between the segments $F\bar{G}$ and $\bar{F}G$. The image of this parallelogram consists of two trapeziums: $G_1F_1A_1\bar{A}_{0,1}$ and its inverse image $\bar{G}_1\bar{F}_1\bar{A}_1A_{0,1}$. These figures lie within $F_0G_0\bar{F}_0\bar{G}_0$ and cover the strange attractor. It is possible to adjust the latter quadrilaterals along their sides $A_1\bar{A}_{0,1}$ and $A_{0,1}\bar{A}_1$, forming a single parallelogram which is $\lambda_+$ times longer (along the unstable direction) and $\lambda_-$ times narrower than $F_0G_0\bar{F}_0\bar{G}_0$. Applying the map once more, four new figures appear as the images of the previous two. These new polygons are nested within the previous ones, forming four pieces of a $\lambda_+^2$

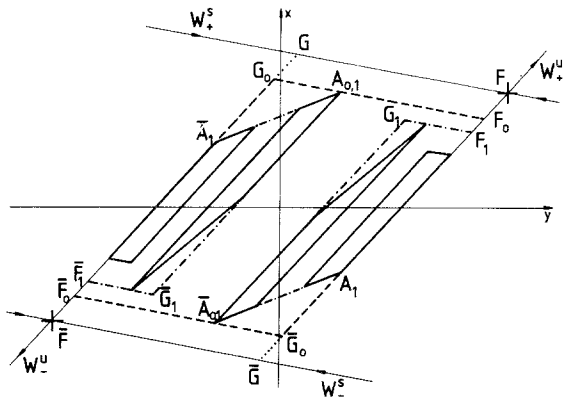


Fig. 8. The coverage of the strange attractor. The figures bounded by dashed, dash-dotted, and continuous bold lines are the strips of the respective covering sets $S_0$, $S_1$, $S_2$. The set $S_i$ is constructed as the image of $S_{i-1}$. Any strip of $S_{i-1}$ contains at most two strips of $S_i$. The strips can be adjusted to form a single parallelogram. During the subsequent steps of the construction the strips contract to the branches of the unstable manifold $W^u_{+-}$ of the period-2 points. The first branches of the stable and unstable manifolds of the fixed points $F$ and $\bar{F}$ are indicated by thin lines.

times longer and $\lambda_-^2$ times narrower parallelogram than the original $F_0G_0\bar{F}_0\bar{G}_0$. Repeating this procedure $n$ times, one can produce a covering set $S_n$ consisting of connected subsets nested within the previous covering set $S_{n-1}$. In the following we shall call these subsets "strips." Since the number of strips, say $q_n$, is at most doubled in every step, $q_n \leqslant q'_n \equiv 2^n$ holds. These pieces can be adjusted to a parallelogram obtained by stretching (shrinking) the original one by a factor of $\lambda_+^n$ ($|\lambda_-|^n$). Thus, the area of $S_n$ is proportional to $\lambda_+^n\,|\lambda_-|^n = |J|^n$. As $n \to \infty$ the subsequent covering sets approach the strange attractor.

Let us denote the width of the strips in the $n$th step by $\varepsilon_n$. The number of squares of size $\varepsilon_n$ needed to cover the strange attractor, $N(\varepsilon_n)$, is equal to the number of squares necessary to cover all the $q_n$ strips of $S_n$. For large $n$ we find

$$(\lambda_+/|\lambda_-|)^n \leqslant N(\varepsilon_n) \leqslant c_1(\lambda_+/|\lambda_-|)^n + c_2 q'_n \tag{A.1}$$

where the coefficients $c_1$ and $c_2$ do not depend on $n$. The left-hand side of (A.1) gives the number of squares needed to cover the adjusted parallelogram in the $n$th step. Since the $q_n$ strips should be covered one by one, the multiple covering of the joint segments has to be taken into account as explained in the caption to Fig. 9. This yields the right-hand side of (A.1), in which the first term dominates since $|\lambda_-| < 1/2$ and $\lambda_+ > 1$.

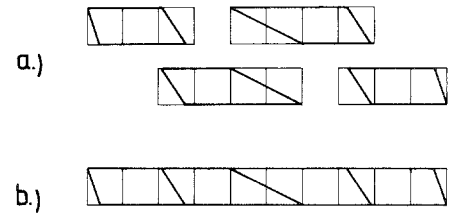


Fig. 9. (a) The number of boxes of size $\varepsilon_2$ needed to cover the four strips of $S_2$ can be obtained by counting (b) twice the boxes covering the joint segments of the adjusted parallelogram. In general, boxes containing parts of $m$ joint segments should be taken into account with multiplicity $m$.

By taking into consideration that $\varepsilon_n \sim |\lambda_-|^n$, the fractal dimension is obtained as

$$D = \lim_{n\to\infty} \frac{\log N(\varepsilon_n)}{\log(1/\varepsilon_n)} = 1 - \frac{\log \lambda_+}{\log |\lambda_-|} \tag{A.2}$$

In other, topologically different cases the same argument can be applied. If $\lambda_-$ is negative, one should start from the "trapping parallelogram" $KL\overline{KL}$ instead of $FG\overline{FG}$ (Fig. 4). Since the expressions as formulated above contain the modulus of $\lambda_-$, they hold for $\lambda_- < 0$ as well.

The formula on the right-hand side of Eq. (A.2) is just the well-known Lyapunov dimension,[38,39] which is equal[40,39] to the information dimension[41] in this system. Moreover, since the probability is uniformly distributed on the strips covering the attractor, the equality of all generalized dimensions[28,42] follows.

To connect with the main idea of this paper, one may ask what happens to the fractal dimension when structural changes of the strange attractor take place. The calculation can be carried out for any other unstable manifold, and the expressions remain unchanged. Therefore, inside the chaotic region, the results obtained for the fractal dimension are the same on both sides of the crisis lines discussed in Sections 3–6.

Equation (A.2) does not hold for the fractal dimension unconditionally if $|\lambda_-| > 1/2$. We have to distinguish the cases when the map restricted to the strange attractor is invertible and when it is not. The invertibility depends on the sign of $\lambda_-$.

*Case 1.* If $\mathrm{sgn}(b) = -\mathrm{sgn}(\lambda_-)$, the map (2.1) is strictly invertible. In this case, although (A.1) is still valid, the second term dominates the rhs, yielding the Lyapunov dimension as a lower limit for $D$ only. Nevertheless, we can formulate a sufficient condition for extending the validity of

Eq. (A.2) to this region, too. Let us suppose that the number of strips $q_n$ scales as $q^n$ with some positive $q$. Then one obtaines

$$N(\varepsilon_n) \approx e_1(\lambda_+/|\lambda_-|)^n + e_2 q^n \tag{A.3}$$

where $e_1$ and $e_2$ are functions of $q$. The stretching ratio is a trivial lower bound for the step-to-step multiplication factor. So, if $q$ lies within the interval $[\lambda_+, \lambda_+/|\lambda_-|]$, the Lyapunov dimension will be preserved, but to decide whether this condition holds, it might be a difficult task and a parameter-dependent problem.

*Case 2.* If $\mathrm{sgn}(b) = \mathrm{sgn}(\lambda_-)$, the map is not invertible. However, if $|\lambda_-| < 1/2$ also holds, the map *restricted to the attractor* is invertible. But the strips containing the pieces of the attractor overlap as soon as $|\lambda_-|$ exceeds 1/2. A strange attractor with overlapping structure is a fat fractal.[43,31] The fractal dimension of the fat attractor is at least the Lyapunov dimension and cannot be greater than the dimension of the phase space:

$$\min\left(1 - \frac{\log \lambda_+}{\log |\lambda_-|}, 2\right) \leqslant D \leqslant 2 \tag{A.4}$$

Although the map has a finite chaotic attractor, due to its overlapping property, the modulus of the Jacobian might exceed 1 (Fig. 2), i.e., $\lambda_+ > 1/|\lambda_-|$. Thus, within a considerable part of the chaotic region of the phase space the fractal dimension is exactly 2. We cannot give an explicit value for $D$ if $\lambda_+ < 1/|\lambda_-|$. Though the results of ref. 44 show that there may exist fat fractals for which the Kaplan–Yorke formula stands, they cannot be taken over, since one of the crucial conditions, $|\lambda_-| < 1/2$, does not hold. We remark, in addition, that the invariant probability distribution supported on the attractor may be a fractal measure[45] with a nontrivial multifractal spectrum.[46] This happens at $\lambda_+ = 2$, $\lambda_- = b = (\sqrt{5} - 1)/2$, where at least the information dimension is found to be different from the fractal dimension.[31]

## APPENDIX B. THE STRUCTURE AND DIMENSION OF THE REPELLOR

Although finite attractors may not appear if $A > A_c(J)$ (as discussed in Section 4), long-term chaotic transients can be observed due to the appearance of a chaotic repellor (more precisely: semiattractor).[34,30,39] In this Appendix we try to illustrate the structure of this strange set and estimate its fractal dimension.

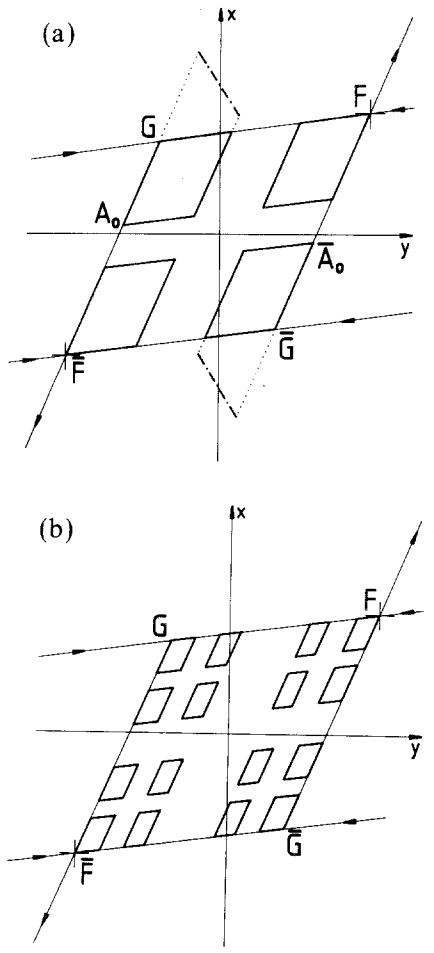


Fig. 10. (a) The first and (b) the second step in constructing the "coarse-grained" repellor in the case of $\lambda_- > \max(0, b)$, when the image of the interval $A_0\bar{A}_0$ (dash-dotted line) lies outside $P_0 \equiv FG\overline{FG}$. The subsequent images (preimages) of this parallelogram are strips lying parallel to the unstable (stable) directions. The intersection of these strips forms a regular double Cantor set.

Due to the properties of the map, if $\lambda_- > 0$ ($\lambda_- < 0$), any bounded invariant set may be situated only in the parallelogram $FG\overline{FG}$ ($KL\overline{KL}$) abbreviated by $P_0$ in the following. Since the repellor $R \subset P_0$ is invariant, i.e., $T^{-n}(R) = T^{-1}(R) = R = T(R) = T^n(R)$ for any $n$, the relations $R \subset P_0$, $R \subset P_1 \equiv T^{-1}(P_0) \cap P_0 \cap T(P_0)$,..., $R \subset P_n \equiv T^{-n}(P_0) \cap P_{n-1} \cap T^n(P_0)$ are satisfied. The nested sequence of $P_n$ approaches $R$ in the limit $n \to \infty$.

This "coarse-grained" construction of the repellor is illustrated on

Fig. 10, in a case where the control parameter $A$ is large enough. [More precisely: we require that if $\lambda_-$ is positive (negative), the whole segment of $A_0\bar{A}_0$ ($C_0\bar{C}_0$) should be mapped out of the parallelogram $P_0$.] This implies that the repellor has a very regular structure: it is the direct product of two Cantor sets. It is known[47,39] that the fractal dimension of a Cartesian product set is the sum of the dimensions of the component sets. By taking into account that the shrinking ratios of the two Cantor sets are $|\lambda_-|$ and $1/\lambda_+$, the dimension turns out to be

$$D = \frac{\log 2}{\log \lambda_+} - \frac{\log 2}{\log |\lambda_-|} \tag{B.1}$$

Figure 11 illustrates the case when the image of the segment $A_0\bar{A}_0$ sticks into $P_0$. This change makes the form of the coarse-grained repellor irregular: it consists of truncated parallelograms now. Thus, there is no hope of determining $D$ directly. However, since the repellor is a proper subset of the double Cantor set with the appropriate shrinking ratios, it is possible to estimate $D$ from above:

$$D \leqslant \frac{\log 2}{\log \lambda_+} - \frac{\log 2}{\log |\lambda_-|} \tag{B.2}$$

This inequality holds if $|\lambda_-| < 1/2$ and $\lambda_+ > 2$. In other cases, since one or both of the one-dimensional component sets of this covering become an interval, the above expression should be modified as shown in Table I.

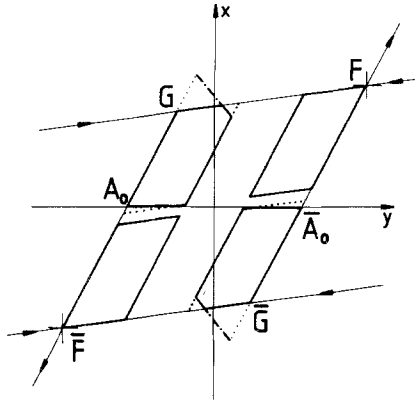


Fig. 11. If the image of $A_0\bar{A}_0$ sticks into $FG\bar{F}\bar{G}$, the set obtained in the first step of the construction of the repellor is a proper subset of the double Cantor structure of Fig. 10a. In subsequent steps the images and preimages of the missing pieces (indicated by dots) lead to further truncations of the regular structure.

**Table I. Results for Fractal Dimension of Repellor and Strange Attractor of the Map (2.1)**

| | $\lvert\lambda_-\rvert < 1/2$ | $1/2 < \lvert\lambda_-\rvert < 1$ |
|---|---|---|
| $A > A_r(J)$ | $D = \log 2/\log \lambda_+ - \log 2/\log \lvert\lambda_-\rvert$ | $D = \log 2/\log \lambda_+ + 1$ |
| $A < A_r(J)$, $A > 2 + J/2$ $(\lambda_+ > 2)$ | $D \leqslant \log 2/\log \lambda_+ - \log 2/\log \lvert\lambda_-\rvert$ | $D \leqslant \log 2/\log \lambda_+ + 1$ |
| $A < 2 + J/2$ $(\lambda_+ < 2)$, $A > A_c(J)$ | $D \leqslant 1 - \log 2/\log \lvert\lambda_-\rvert$ | $D \leqslant 2$ |
| $A < A_c(J)$, $A > 1 + J$ $(\lambda_+ < 1)$ (strange attractor) | $D = 1 - \log \lambda_+/\log \lvert\lambda_-\rvert$ | $\min(1 - \log \lambda_+/\log \lvert\lambda_-\rvert, 2) \leqslant D \leqslant 2$ |

The lower bound of that region of the parameter plane where the repellor has a regular double Cantor structure with the dimension (B.1) is denoted by $A_r(J)$ on Fig. 2. In the parameter region $A_r(J) > A > A_c(J)$, between the regular double Cantor set structure and the boundary crisis of the strange attractor, a crossover takes place in the dimension of the repellor from (B.1) to (A.2). The crossover region disappears only if $\lambda_- = b$, in the special case when (2.1) is equivalent to the generalized baker's transformation. $A_r(J)$ can be derived from the condition that the images of the $x$-axis piece $A_0\bar{A}_0$ (or $C_0\bar{C}_0$ of Fig. 4 if $\lambda_- < 0$) just touch from outside the stable manifold of the fixed points. The equations for $A_r(J)$ turn out to be the continuation of the curves of $A_c(J)$ beyond the chaotic region.

## ACKNOWLEDGMENTS

We are indebted to Z. Kaufmann and to Z. Rácz for their critical reading of the manuscript and to M. Mareyen for drawing our attention to ref. 4. This work was supported by grants of the Hungarian Academy of Sciences AKA 283.161 and OTKA 819.

## REFERENCES

1. S. Coleman, in *Secret Symmetry: An Introduction to Spontaneous Symmetry Breakdown and Gauge Fields in Laws of Hadronic Matter*, E. Zichichi, ed. (Academic Press, New York, 1975); D. Forster, *Hydrodynamic Fluctuations, Broken Symmetry and Correlation Functions* (Benjamin, Reading, 1975); S. K. Ma, *Modern Theory of Critical Phenomena* (Benjamin, Reading, 1976).
2. N. Morioka and T. Shimizu, *Phys. Lett.* **66A**:447 (1978); J. Shimida and T. Nagashima, *Prog. Theor. Phys.* **61**:1605 (1979); K. H. Alfsen and J. Froyland, *Physica Scripta* **31**:15 (1985).

3. E. N. Lorenz, *J. Atmos. Sci.* **20**:130 (1963).
4. M. Kitano, T. Yabukazi, and T. Ogawa, *Phys. Rev. A* **29**:1288 (1984).
5. C. Grebogi, E. Ott, and J. A. Yorke, *Physica* **7D**:181 (1983).
6. P. Collet and J.-P. Eckmann, *Iterated Maps on the Interval as Dynamical Systems* (Birkhäuser, Boston, 1980).
7. T. Rikitake, *Proc. Camb. Phil. Soc.* **54**:89 (1958).
8. O. E. Rössler, *Z. Naturforsch.* **31a**:1664 (1976).
9. J. A. Yorke and E. D. Yorke, *J. Stat. Phys.* **21**:263 (1979).
10. A. Arneodo, P. Coullet, and C. Tresser, *Phys. Lett.* **81A**:197 (1981).
11. C. Sparrow, *The Lorenz Equations: Bifurcation, Chaos and Strange Attractors* (Springer, New York, 1982).
12. D. V. Lyubimov and M. A. Zaks, *Physica* **9D**:52 (1984).
13. P. Szépfalusy and T. Tél, *Physica* **16D**:252 (1985).
14. J.-M. Gambaudo, I. Procaccia, S. Thomae, and Ch. Tresser, *Phys. Rev. Lett.* **57**:925 (1986); I. Procaccia, S. Thomae, and C. Tresser, *Phys. Rev. A* **35**:1884 (1987).
15. L. P. Shilnikov, *Math. USSR Sb.* **6**:427 (1968).
16. Z. Kaufmann, P. Szépfalusy, and T. Tél, *Acta Phys. Hung.* **62**:321 (1987).
17. R. Lozi, *J. Phys.* (Paris) **39**:C5-9 (1978); R. Lozi, in *Intrinsic Stochasticity in Plasmas*, G. Laval and D. Gresillon, eds. (Edition de Physique, Orsay, 1979).
18. M. Hénon, *Commun. Math. Phys.* **50**:69 (1976).
19. M. Misiurewicz, in *Nonlinear Dynamics*, R. H. G. Helleman, ed. (New York Academy of Sciences, New York, 1980).
20. T. Tél, *Z. Phys. B* **49**:157 (1982); *Phys. Lett.* **94A**:334 (1983); *J. Stat. Phys.* **33**:195 (1983).
21. P. Collet and M. Levy, *Commun. Math. Phys.* **93**:461 (1984).
22. G. Gunaratne, Thesis, Cornell University, Ithaca, New York (1986); H. Hato, T. Morika, K. Tomita, and H. Mori, *Prog. Theor. Phys.* **78**:721 (1987); D. Auerbach, B. O'Shaughnessy, and I. Procaccia, *Phys. Rev. A* **37**:2234 (1988); P. Cvitanović, G. Gunaratne, and I. Procaccia, *Phys. Rev. A*, to appear.
23. R. Thibault, *Comptes Rendus* **297**(Ser. 1):603 (1983); R. L. Devaney, *Physica* **10D**:387 (1984).
24. T. Tél, *Phys. Lett.* **97A**:219 (1983).
25. R. Riedi, Thesis, Zürich (1986).
26. E. Ott, *Rev. Mod. Phys.* **53**:655 (1981).
27. J. D. Farmer, E. Ott, and J. A. Yorke, *Physica* **7D**:153 (1983).
28. H. G. E. Hentschel and I. Procaccia, *Physica* **8D**:435 (1983).
29. R. Badii and A. Politi, *Phys. Rev. Lett.* **52**:1661 (1984).
30. P. Szépfalusy and T. Tél, *Phys. Rev. A* **34**:2520 (1986).
31. J. C. Alexander and J. A. Yorke, *Ergod. Theor. Dynam. Syst.* **4**:1 (1984).
32. H. Fujisaka and S. Grossmann, *Z. Phys. B* **48**:261 (1982); J. Nierwetberg, Thesis, Regensburg (1985).
33. J. Wilbrink, *J. Phys. A* **19**:2973 (1986).
34. H. Kantz and P. Grassberger, *Physica* **17D**:75 (1985).
35. C. Chen, G. Györgyi, and G. Schmidt, *Phys. Rev. A* **35**:2660 (1987).
36. J. A. Ketoja, Helsinki University of Technology Report TKKF-F-B109 (Helsinki, 1987).
37. B. B. Mandelbrot, *Fractals: Form, Chance and Dimension* (Freeman, San Francisco, 1977).
38. J. L. Kaplan and J. A. Yorke, in *Lecture Notes in Mathematics*, No. 730 (1979), p. 223.
39. J.-P. Eckmann and D. Ruelle, *Rev. Mod. Phys.* **57**:617 (1985).
40. L.-S. Young, *Ergod. Theor. Dynam. Syst.* **2**:109 (1982).
41. J. Balatoni and A. Rényi, *Publ. Math. Inst. Hung. Acad. Sci.* **1**:9 (1956) (in Hungarian) [English translation in *Selected Papers of A. Rényi*, Vol. 1, P. Turán, ed. (Akadémiai,

Budapest, 1976), p. 558]; A. Rényi, *Acta Math. Hung.* **10**:193 (1959); A. Rényi, *Probability Theory* (North-Holland, 1970).
42. P. Grassberger, *Phys. Lett.* **97A**:227 (1983).
43. D. Farmer, *Phys. Rev. Lett.* **55**:321 (1985); in *Dimensions and Entropies in Chaotic Systems*, E. Mayer-Kress, ed. (Springer, New York, 1986), p. 54.
44. K. J. Falconer, *J. Stat. Phys.* **47**:123 (1987).
45. D. Farmer, *Z. Naturforsch.* **37a**:1304 (1982).
46. T. C. Halsey, M. H. Jensen, L. P. Kadanoff, I. Procaccia, and B. I. Shraiman, *Phys. Rev. A* **33**:1141 (1986).
47. P. Grassberger, in *Chaos*, A. V. Holden, ed. (Manchester University Press, Manchester, 1986).